Supporting Information

Roper et al. 10.1073/pnas.1220842110

SI Text

I. Modeling Genetic Composition of a Small Nuclear Population

We estimate the number of nuclei needed to populate a single hyphal tip by two methods: (*i*) Ramos-Garcia et al. (1) use confocal microscopy to measure hyphal tip extension rates in mature *Neurospora crassa* colonies. They measure average tip growth rate of 0.14 μm·s^{-1}; assuming a nuclear division time of 100 min (2), it follows that 840 μm of hypha [or ∼130 nuclei, assuming a nuclear density of 1.5 nuclei/10 μm of hypha (1)] are needed to supply each growing hyphal tip. However, fungi growing under microscopic observation usually grow at suboptimal rates [e.g., race tube measurements give growth rates of 0.8 μm·s^{-1} (3)]. (*ii*) Accordingly, we also estimate the nuclear population needed to sustain a tip by indirect methods. Our velocimetry (Fig. 3*A*) shows that the growing edge of a mature colony is fed by nuclear flows extending 20 mm into the colony. Because fusions create a multiconnected path from the colony interior to its edge, the precise distribution of nuclei to tips is not straightforward. However, hyphae of *soft* (*so*) colonies do not fuse, creating a tree-like hyphal network, and *so* has very similar growth rates (4) and mean nuclear velocities (Fig. 3*A*) to those of wild-type mycelia. Moreover, nuclear flow within the *so* network is restricted to a small number of leading hyphae. We estimated that each hypha feeds 20 growing hyphal tips. It follows that of the 20 mm of leading hypha, 1 mm of nuclei must produce enough progeny, by mitosis, to populate each tip. Accounting for the density of nuclei we observed in leading hypha (3 nuclei per 10 μm, e.g., Movie S2), we arrive at a comparable estimate (300 nuclei) for the number of nuclei needed to populate a single tip. We note that this population size is probably large for a filamentous fungus, reflecting *N. crassa*'s rapid growth. For example, *Fusarium oxysporum* germlings have only a single mitotically active nucleus per hyphal tip (5).

How would genetic diversity evolve within each hypha in the absence of nuclear mixing? As a null model for the population evolution, we model the division of a group of 130 genetically mixed nuclei at the hyphal tip by a Moran process (6, 7). We discover that the richness of the apical population decreases exponentially with time: Simulated hyphae show loss of genetic richness and even total homogenization. Specifically we model the dynamics of a population of N nuclei that contains two distinguishable nucleotypes ("red" and "green") as a two-species population (7). We assume that nuclei divide independently and at random with mean interdivision time τ (Fig. S1*A*). When a division occurs, a single nucleus picked at random from among the dividing population divides into two identical copies. To maintain the fixed size of the population, a second nucleus picked at random from the original population is removed from the population: We consider such nuclei as being left behind in a subapical compartment, while the rest of the dividing population advances with the hyphal tip. If we denote the number of red (i.e., *hH1-DsRed* transformed) nuclei by n_r, then n_r performs a random walk on the set $\{0, 1, \ldots, N\}$. Then if the population's genetic diversity is measured by the heterozygosity, H_k after k nuclear divisions, i.e., the probability that two randomly selected nuclei have different nucleotypes, $H(n_r) = 2n_r(N - n_r)/N^2$, it can be easily shown that $\mathbb{E}(H_{k+1}|H_k) = (1 - 2/N^2)H_k$. If we define a generation time for the system (the length of time taken for each nucleus to divide once, on average) by $\tau_g = N\tau \approx 100$ min, then at time t, then in the limit of large N, the expected heterozygosity of the system is given by $H(t) = H(0)\exp(-2t/N\tau_g)$ (Fig. S1*B*), i.e., decays exponentially with the distance grown by the colony. By contrast, our measurements in real *N. crassa* heterokarya show that diversity, sampled over 130 nuclei drawn from the hyphal tips, increases as the colony grows. It follows that additional nuclear dynamics, missing from the Moran model, exist within real *N. crassa* colonies.

II. Defining an Index of Mixing for Heterokaryotic Colonies

We use std(p_r)—the SD in the proportion, p_r, of hH1-DsRed–labeled nuclei between samples of 130 nuclei taken from the hyphal tips of the colony—as an index of how well mixed the two nucleotypes are. We choose 130 nuclei as the minimum number of nuclei necessary to fill the space continually created at a growing tip (*SI Text*, *section I*). The rationale for choosing std(p_r) as a measure of mixing is that if the nucleotypes are perfectly well mixed, then the nuclei in the sample should have independent nucleotypes. Thus, in a sample of N_{nucl} nuclei, we expect $\text{std}(p_r) \sim 1/\sqrt{N_{nucl}}$, i.e., to go to zero as the sample size is increased. In fact, std(p_r) seems to asymptote to a constant value as N_{nucl} is increased (representative data for one growth stage are shown in Fig. S2). std(p_r) not decaying to zero as N_{nucl} is increased indicates that nuclei are not well mixed, and we use std(p_r) as an index of the quality of mixing, with smaller values indicating better mixing. An explicit comparison of the p_r distributions between well-mixed and unmixed chimeras is shown in Fig. 4*E*. Note also that std(p_r) varies only weakly with N_{nucl}, so our mixing index is not affected by uncertainty in the number of nuclei needed to populate each tip.

III. Measuring Nuclear Dispersal in Wild-Type and *so* Colonies

A. Controlling for the Number of Labeled Spores Inoculated into the Colony. We performed a control experiment to test that introducing large numbers (∼75,000 spores) of *hH1-gfp* conidia into wild-type colonies did not strongly affect the network and nuclear flows within the colony. One-dimensional colonies were grown following the protocol in the main text; i.e., one edge of a 40 × 50-mm agar block was inoculated with 6 μL of wild-type spores ($\sim 6 \times 10^5$ spores). Once the colony edge had advanced 20 mm, a 0.75-μL droplet of *hH1-gfp* spores was inoculated into the colony, 4 mm behind the colony edge. We prepared conidial suspensions at different concentrations, to vary the number of spores introduced into the colony from 750 spores to 75,000 spores. The conidial suspensions were prepared 24 h before their inoculation into the unlabeled colony. Conditioning spores by storing them overnight in deionized water was found to increase the rate of fusion between spores and unlabeled colony, particularly when spores were inoculated into *so* colonies (main text). For all droplets assayed, the first fusions were observed 4 h after inoculation. We measured the distributions of nuclei within the colony 5 h after inoculation (i.e., 1 h following the first fusion), using a Zeiss SteREO Discovery V12 fluorescence stereomicroscope with a motorized stage, visualizing the colony at 33× magnification, with a 10× long working distance M2BIO front lens. Nuclear densities (number of nuclei per area) were measured on transects perpendicular to the direction of growth, using a combination of manual counting of nuclei, or, when nuclear densities were too large for nuclei to be counted manually, using automated image analysis. We measured the mean and maximal distance that nuclei traveled into the colony. Measurements were consistent across three replicates at each concentration. We

found that nuclei dispersed rapidly through the colony even at the lowest concentration of spores (750 spores) (Fig. S3), proving that rapid nuclear dispersal is not a result of reconfiguration of the hyphal network in response to encountering the labeled spores.

B. Comparing Nuclear Dispersal Between *so* and Wild-Type Colonies. Although nuclei introduced into *so* colonies disperse as rapidly through the colony from the sites of their introduction as in wild-type colonies (Fig. 4*A*), we noted (representative micrographs in Fig. S4) that nuclei moving through the *so* colony remain closely packed together, whereas in wild-type colonies nuclei became spread apart from each other during their transport through the hypha. This observation inspires a mathematical model (main text and *SI Text*, *section VIII*) for how the velocity field created by fusions causes sibling nuclei to arrive at the growing tips at well-separated times.

IV. Measuring Nuclear Kinematics

A. A Hybrid Particle Image Velocimetry–Particle Tracking Method. Under our fluorescence imaging (our microscopy setup is described in the main text, *Materials and Methods*) nuclei appear as bright spots. The displacements of spots between frames (typically the time lapse between image captures is between 0.1 and 0.5 s) allows us to calculate nuclear velocities. There are two commonly used techniques for determining particle displacements. Particle imaging velocimetry (PIV) treats the bright spots as tracers of an underlying coherent velocity field and computes cross-correlations of small windows of the image to assign velocity fields. Nearby nuclei are assumed to be moving coherently (i.e., with similar speeds), and individual nuclei do not need to be tracked. Conversely, particle tracking (PT) explicitly identifies spots between frames and allows measurement of individual nuclear velocities. However, it is less effective when, as here, the bright spots are dense enough, or their velocity is large enough, that the distance traveled by a spot between frames is comparable to or greater than the spacing of spots. We developed a method that hybridizes these two techniques to obtain individual nuclear velocities for fields containing up to 10^4 nuclei. First, we used the PIV code MatPIV (8) to extract the PIV data. Then we used a modified version of the particle locating method of Grier and Crocker (9) to identify the movements of individual particles between frames. Specifically, we used high and low pass filters to remove pixel noise and subtract background brightness of the hyphae, reducing the image to bright spots on a uniformly dark background. Nuclei were identified by thresholding this image using Otsu's method and then characterized by their size and brightness-over-background. Because nuclei were only a few pixels across, we found that the method of Grier and Crocker, which finds the centers of bright spots as the intensity weighted centroid of a masked area of the image, produced pixel-locked displacements. Instead, we used cubic splines to interpolate the intensities and locate the brightest spot in each nucleus to subpixel precision.

Given a particle number i, location $\boldsymbol{x}_i^{(1)}$, size $r_i^{(1)}$, and total intensity $I_i^{(1)}$ in the first frame, our hybrid PIV-PT scheme interpolates the gridded velocity field obtained from the PIV scheme as an initial guess for the particle displacements $\boldsymbol{u}_i^*$. We then compute the particle displacement between frames by performing a greedy minimization over all particle data in the second frame $(\boldsymbol{x}_j^{(2)}, r_j^{(2)}, I_j^{(2)})$, the quantity

$$\left\|\boldsymbol{x}_j^{(2)} - \boldsymbol{x}_i^{(1)} - \boldsymbol{u}_i^*\right\|^2 + \alpha\left(r_j^{(2)} - r_i^{(1)}\right)^2 + \beta\left(I_j^{(2)} - I_i^{(1)}\right)^2 \qquad \text{[S1]}$$

that finds the nucleus in the second frame whose displacement from i most closely matches the displacement predicted from the PIV data, while also remaining consistent in size and brightness. Empirically we find that any small values for the parameters α and β produce robust nuclear tracking: In these analyses we used $\alpha = 0$ and $\beta = 0.001$. Working at 10× magnification, our hybrid PIV-PT algorithm produces simultaneous and accurate measurements of particle velocities for fields containing up to 10^4 nuclei (Fig. S5).

B. Correcting for Finite Focal Thickness. We find that the number density of nuclei (n_ℓ) observed in unit length of any hypha increases in direct proportion with the hyphal diameter d [rather than with its cross-sectional area (Fig. S6)], which is what we would expect if the nucleocytoplasmic volume fraction were independent of the hyphal dimensions. We interpret this to mean that we are collecting light only over a fixed thickness, λ of hypha: The measured number is therefore related to the number density of nuclei per unit volume, n_v by $n_\ell = \lambda d n_v$. Other nuclei may be out of focus or obscured behind other bright nuclei. Thus, when measuring the true number of nuclei per unit hyphal length (e.g., to calculate the flux in the hypha), we correct by multiplying n_ℓ by the diameter of the hypha. Although correction allows the relative fluxes between hyphae to be observed, it means that individual flux measurements include the unknown length scale λ.

C. Hyphal Growth Under Microscopic Observation Is Suboptimal. During all of our experiments *N. crassa* colonies were incubated at 25 °C in constant light. Under these conditions we obtained growth rates of $\sim 3\ \text{mm}\cdot\text{h}^{-1} = 0.8\ \mu\text{m}\cdot\text{s}^{-1}$, consistent with previous measurements (3). However, tip growth velocities measured during fluorescence microscopy were significantly slower [$0.24 \pm 0.002\ \mu\text{m}\cdot\text{s}^{-1}$ (mean ± SE) based on 708 tips measured over three different colonies]. The mean growth rate of $0.14\ \mu\text{m}\cdot\text{s}^{-1}$ previously reported by Ramos-Garcia et al. (1) is also significantly less than the optimal colony growth rate. Fluorescence microscopy apparently provides suboptimal conditions for hyphal growth. We expect that the increased growth rate for optimally growing colonies will create increased mean nuclear velocities (Figs. 3 and 5) and fluxes (Fig. 4) over our measurements. For this reason, we compare rates of nuclear dispersal (Figs. 2*B* and 4*A*) during optimal growth with the maximum hyphal growth rate, rather than with the nuclear velocities that we measured experimentally.

V. Distinguishing Nucleotypes and Genotypes

Because the mRNAs coding for the labeled histones must travel from the nuclei to sites of translation in the cytoplasm, and because histones can then diffuse through the cytoplasm before being taken up by a nucleus, nucleotypes (i.e., DsRed/GFP fluorescence levels) become gradually decoupled from the nuclear genotypic identities as nuclei take up heterogeneously labeled histones from the surrounding cytoplasm. In fact, we found that as a colony increases in size, not only were heterotypic nuclei created (i.e., containing both hH1-GFP and hH1-DsRed labels), but also the relative proportion of homotypic hH1-GFP–labeled nuclei appeared to increase. Because homokaryotic hH1-GFP colonies and hH1-DsRed colonies have the same rates of growth and both labeled histones were under the Pccg-1 promoter, we do not believe this to be a result of differential rates of mitosis between the two nuclear genotypes or of different rates of production of the labeled histones: Rather, DsRed appears to be gradually sequestered into cell vacuoles (although we are not able to determine whether this sequestration is preceded by cleavage of the fluorophore from the histone). Thus, real-time imaging of the dynamics of nuclear populations within chimeric *N. crassa* mycelium monitors only nucleotypic mixing, and we cannot infer the underlying genotype abundances. Diffusion of labeled histones between nuclei may account for some of the increase in observed well-mixedness with time.

Fluorescence of conidia, the asexual spores of the colony, is a reliable indicator of genotype distributions within the colony. To test this, we harvested spores from a 7-d-old heterokaryon and measured spore fluorescence for ~1,000 spores by imaging at 40× with an upright microscope (main text, *Materials and Methods*), categorizing spores as homokaryotic hH1-DsRed/homokaryotic hH1-GFP/heterokaryotic. We then plated out conidia on sorbose media [1× Vogels salts, 0.4% sucrose, 0.8% D-sorbose, and 1.5% (wt/vol) agar] and measured the proportions of homokaryotic or heterokaryotic colonies produced. Although it is possible that, e.g., a genetically homokaryotic hH1-GFP conidium may contain enough residual hH1-DsRed to appear to be heterokaryotic, it is unlikely that a colony grown from this conidia would have significant dsRed fluorescence. Accordingly, we use the identity of the colonies as an estimate of the true genetic identity of the spores. We found that fractions of the three different categories were statistically indistinguishable between spore measurements and colony measurements of nucleotype identity (Table S1).

Conidial abundances therefore allow measurement of the fractions of genotypes in a heterokaryotic colony, but with the disadvantage that evolution of genotypic fractions cannot be tracked before conidiation. To measure conidial genotypes we scraped conidial chains from a colony, using a hypodermic needle, and dipped the needle into a water droplet on a slide. The hydrophobicity of the spores drives the conidial chains off the needle, and many spores disassociate. We imaged intact fragments: chains of at least five spores. Imaging these chains at 40× magnification (main text, *Materials and Methods*) we can both count the number of nuclei in the spore and categorize spores into the categories above. We then computed the maximum-likelihood estimate for p_r (the probability that a nucleus has a *hH1-DsRed* genotype) for each conidial chain, assuming that each nucleus in the chain is drawn independently and at random. In fact, the work of Atwood and Mukai suggests that nucleotypic proportions in conidiophores are slightly overdispersed (10), so that there are fewer heterokaryotic conidia than would be expected under this model, so we test for consistency that our likelihood maximization produces close to the observed proportion of conidia in all three categories. Our measurements (maintext, Fig. 1*C*) show that the well-mixedness of genotypes within conidiophores, $\mathrm{std}(p_r)$ is very close to the value obtained by measuring nucleotypes within the mycelium ($\mathrm{std}(p_r) = 0.09$), suggesting that nucleotypes and genotypes are distributed statistically similarly through the colony.

VI. Calculation of and Optimization of p_{mix} in Colonies That Lack Hyphal Fusion

A. Random Branching Colonies. To model random branching, we consider the branching of an individual hypha as a Poisson process, so that the interbranch distances are independent exponential random variables with mean λ^{-1}. Then if we denote by $p_k(x)$ the probability that exactly k hyphae have been produced (i.e., $k-1$ branching events occur) over a distance x of leading hyphal growth, then the $\{p_k\}$ satisfy master equations:

$$\frac{dp_k}{dx} = (k-1)\lambda\, p_{k-1} - k\lambda\, p_k. \qquad \textbf{[S2]}$$

To solve these equations, we introduce a generating function $G(x,\xi) = \sum_k p_k(x)\xi^k$. In terms of this function, the complete set of master equations can be written as a single linear hyperbolic partial differential equation on G:

$$\frac{\partial G}{\partial x} - \lambda\xi(\xi-1)\frac{\partial G}{\partial \xi} = 0. \qquad \textbf{[S3]}$$

We can solve this equation by the method of characteristics, obtaining $G(x,\xi) = \xi/(\xi-(\xi-1)e^{\lambda x})$. By expanding G as a power series in ξ we obtain explicit expressions for each of the likelihoods, p_k: $p_k(x) = e^{-\lambda x}(1-e^{-\lambda x})^{k-1}$; i.e., the p_k have a geometric probability distribution with parameter $e^{-\lambda x}$. Suppose we examine the colony at some distance x between the first branching of the leading hypha $x=0$ and the mycelial edge $x=x_2$. Because hyphae divide randomly and independently in this model, the distribution of tips fed by a hypha at any distance x from the first branch point (and distance x_2-x from the hyphal tips) is $p_k(x_2-x)$. The likelihood that any randomly chosen hypha feeds exactly k tips is $P_k = \int_0^{x_2}\langle k(x)\rangle p_k(x_2-x)\,\mathrm{d}x / \int_0^{x_2}\langle k(x)\rangle \mathrm{d}x$, where $\langle k(x)\rangle \equiv \sum_k k p_k(x) = e^{\lambda x}$ is the average number of hyphal tips fed by a leading hypha that grows a distance x. Inputting the known geometric distribution for $p_k(x)$, we can evaluate these integrals:

$$P_k = \frac{\left(1-e^{-\lambda x_2}\right)^k\left(ke^{-\lambda x_2}+1\right)}{k(1+k)}. \qquad \textbf{[S4]}$$

It follows that if $\lambda x_2 \gg 1$ (i.e., the original leading hypha feeds a large number of tips), then $P_k \sim 1/k(k+1)$. Then the likelihood of a pair of nuclei being delivered to different tips is

$$p_{\mathrm{mix}} = 1 - \sum_k P_k/k = 2-\pi^2/6 \approx 0.355. \qquad \textbf{[S5]}$$

To generate numerical data for p_{mix} for a colony with a biologically reasonable number of tips, we performed stochastic simulations, in which the hyphal branching pattern was determined by allowing a colony with n branches to grow an $Exp(1/n\lambda)$ distance, and then one of the n branches was picked at random with equal probabilities and split into two branches. We found that for a colony with 100 tips the average value for $p_{\mathrm{mix}} = 0.368$, close to the asymptotic value given by Eq. **S5**.

B. Colonies with Organized Branching. The geometry of a branching tree in which the interbranch distances are prescribed is completely specified by the sequence of hyphae that branch. We therefore search for optimally branching trees by searching over a space of sequences $\{x_i : i = 1,2,\cdots N-1 \text{ and } x_i \in \{1,2,\ldots,i\}\}$, where N is the total number of tips fed by the entire branching structure. Starting from a randomly generated branching sequence, we use a Monte Carlo method to iteratively minimize p_{mix} by sweeping through the indexes i and generating new values of x_i. Although this method rapidly converges to a local minimum value of p_{mix} that cannot be improved by changing any single branch x_i, we found multiple local minima, all close to the global minimal value of p_{mix}. The existence of a manifold of local optima seems to result from p_{mix} minimization only weakly constraining the branching sequence in the interior of the colony, while stringently constraining the branching points closest to the colony periphery and the relative lengths and numbers of hyphae feeding one, two, or three tips only (Fig. S7).

We argue in the main text that the maximum value of p_{mix} occurs when for each value of x, each hypha located at distance x downstream of the leading hypha feeds the same number of tips. Equidistribution is possible only when the total number of hyphal tips, N is large. Under the equidistribution assumption, the probability of the sibling nuclei produced by a mitosis at distance x feeding into different tips is $1-m/N$, where m is the number of hyphae at position x. Then on averaging over all nuclei at all stations (noting that the range of x-values over which the colony contains exactly m hyphae is $\propto 1/m$) we obtain

$$p_{\mathrm{mix}} = \frac{\sum_{m=1}^{N}\left(1-\frac{m}{N}\right)}{\sum_{m=1}^{N}1} = 1-\frac{N(N+1)}{2N^2} \sim \frac{1}{2}; \qquad \textbf{[S6]}$$

i.e., a large tree with many branches must have mixing probability that is asymptotically no greater than $\frac{1}{2}$, consistent with our numerical simulations.

VII. Taylor Dispersion Is Weak Within Individual Hyphae

The long time mixing of a solute flowing through a capillary network is dominated by Taylor dispersion within individual capillaries. Applying Saffman's model (11) (which does not include differences in hyphal cross-sections or interbranch distances), we would expect this Taylor dispersion to generate large enough variation in the time of delivery of sibling pairs of nuclei to the growing edge of the colony to ensure that they do not arrive at the same hyphal tip (main text). However, velocity profiles within hyphae are very different from flows in capillaries. Nuclear movements have a large random component, suggestive of frequent collisions with septa, other nuclei, and other organelles. To accurately extract mean flow profiles across the hyphal cross-section we averaged a large number of individual nuclear velocity measurements N_{nucl} collected from N_{hyph} different measurements. When nuclear velocities were scaled by the extrapolated centerline velocity within the hypha, and distances from the centerline scaled by the hyphal radius, we obtained a universal dependence of the (time and axially averaged) velocity v upon radial position r : $v = 1 - r^2/(1+2\Lambda)^2$ (Fig. S8*B*). The parabolic dependence of velocity upon the radial coordinate is consistent with Poiseuille flow in which friction between the hyphal walls and cytoplasm resists the pressure driving the flow. However, our measured nuclear velocities do not decrease to zero at the hyphal wall. Instead, there is effective hydrodynamic slip on the wall (12) that we can effectively parameterize as being associated with a slip length, λ equal to 0.2 × the hyphal diameter. (Our resolution of the distance between nuclei and the hyphal wall is not high enough to determine whether this slip length truly scales with the hyphal diameter or whether there is also a minimum slip length associated with the narrowest hyphae.) We can only speculate at the physical origins of this slip length—whether crowding from organelles prevents nuclei from touching the hyphal walls or whether a combination of the mobility of molecules in the hyphal cell membrane and nuclear envelope allows the two to slide past each other when there is contact. Nonetheless, nuclei were also much more concentrated at the center of the hypha than near hyphal walls (Fig. S8*A*), occupying typically the central 60% of the hypha, probably because of crowding from other organelles and vacuoles at the walls. From the combination of these two effects, the total velocity difference between innermost and outermost nuclei is only 25% of the total velocity difference across an equivalently sized capillary, and because changes in solute velocity as a particle diffuses across the cross-section of a capillary drive its downstream dispersion, dispersion is much weaker also. Quantitatively, we can reproduce the analysis of Taylor (13) to compute the hydrodynamic dispersion in the presence of slip and nuclear confinement (here we follow a multiple-scales argument originating with Jonathan Mestel, rather than Taylor's original analysis).

On defining cylindrical polar coordinates (r,z), with the z axis along the axis of the hypha, the time-averaged axial velocity in a hypha with diameter a is equal to $\boldsymbol{u} = u(r)\boldsymbol{e}_z$, where $u(r) = \frac{2\overline{U}}{2-\chi^2+4\Lambda}(1 + 2\Lambda - r^2/a^2)$, $\Lambda = \lambda/a$ is the nondimensionalized slip length, nuclei are confined to a region $0 < r < \chi a$ of the hypha, and $\overline{U}$ is the axial velocity averaged over this region. If the probability of locating a single nucleus in an annulus $r \in (r', r'+dr)$ and $z \in (z', z'+dz)$ is $p(r,z)drdz$, then the probability density function $p(r,z,t)$ evolves with time according to the advection–diffusion equation

$$\frac{\partial p}{\partial t} + u(r)\frac{\partial p}{\partial z} = D\left(\frac{1}{r}\frac{\partial}{\partial r}\left(r\frac{\partial p}{\partial r}\right) + \frac{\partial^2 p}{\partial z^2}\right), \qquad \textbf{[S7]}$$

where D is the diffusivity of the single nucleus. Three effects lead to nuclear diffusion: Brownian motion, nuclear translocation by molecular motors, and random collisions of nuclei with each other and with other organelles within the cytoplasm. Because nuclei are relatively large objects (~3 μm), we expect the last two effects to dominate. In the slow flows of nuclei near hyphal tips ($\overline{U} \approx 0.1$ μm·s^{-1}) motor-driven movement is already known to be the major correction to bulk cytoplasmic transport (1), but in the faster flows that we observe in leading hyphae ($\overline{U} \approx 1-5$ μm·s^{-1}), we expect that collisions that produce a diffusivity $D \sim \overline{U}\ell$, where ℓ is the mean intercollision distance (we estimate $\ell \approx 3-10$ μm from images of vacuoles and other large organelles within a hypha), may become dominant. We follow Mestel by separating p into cross-sectional average and r-varying contributions: $p(r,z,t) = \overline{p}(z,t) + p'(r,z,t)$, where $\overline{p}$ is the cross-section average of the probability density function. Then, denoting cross-section averages by overbars, we can average the entire Eq. **S7** to obtain

$$\frac{\partial \overline{p}}{\partial t} + \overline{U}\frac{\partial \overline{p}}{\partial z} + \overline{u(r)\frac{\partial p'}{\partial z}} = D\frac{\partial^2 \overline{p}}{\partial z^2}. \qquad \textbf{[S8]}$$

Subtract Eq. **S8** from Eq. **S7** and break p up into average and r-varying contributions to obtain

$$\frac{\partial p'}{\partial t} + u(r)\frac{\partial p'}{\partial z} - \overline{u(r)\frac{\partial p'}{\partial z}} + \left(u(r) - \overline{U}\right)\frac{\partial \overline{p}}{\partial z} = D\left(\frac{1}{r}\frac{\partial}{\partial r}\left(r\frac{\partial p'}{\partial r}\right) + \frac{\partial^2 p'}{\partial z^2}\right). \qquad \textbf{[S9]}$$

For a long, narrow hypha, length L, we expect diffusion in the r direction to be a factor L^2/a^2 stronger in this equation than diffusion in the z direction. Under this strong radial diffusion, after a time $t \gtrsim a^2/D$, the nucleus will have diffused across the entire cross-section of the hypha, making its distribution in r close to (but not identically) uniform: It follows that $|p'| \ll \overline{p}$, so the dominant balance in this equation is between the terms:

$$\left(u(r) - \overline{U}\right)\frac{\partial \overline{p}}{\partial z} = \frac{D}{r}\frac{\partial}{\partial r}\left(r\frac{\partial p'}{\partial r}\right). \qquad \textbf{[S10]}$$

We can integrate this equation to obtain an expression relating p' to the axial gradient in $\overline{p}$:

$$p' = \frac{\overline{U}}{4(2+4\Lambda-\chi^2)D}\left(\chi^2 r^2 - \frac{r^4}{2a^2} - \frac{\chi^4 a^2}{3}\right) \qquad \textbf{[S11]}$$

(We use $\overline{p'} = 0$ to obtain the constant term, above). We may then substitute for the subdominant terms $\overline{u(r)\frac{\partial p'}{\partial z}}$ in Eq. **S9**,

$$\overline{u(r)\frac{\partial p'}{\partial z}} = -\frac{\overline{U}^2 a^2 \chi^8}{48D(2-\chi^2+4\Lambda)^2}\frac{\partial^2 \overline{p}}{\partial z^2}, \qquad \textbf{[S12]}$$

to obtain a one-dimensional (1D) advection–diffusion equation for $\overline{p}$:

$$\frac{\partial \overline{p}}{\partial t} + \overline{U}\frac{\partial \overline{p}}{\partial z} = D\left(1 + \frac{\overline{U}^2 a^2 \chi^8}{48D^2(2-\chi^2+4\Lambda)^2}\right)\frac{\partial^2 \overline{p}}{\partial z^2}. \qquad \textbf{[S13]}$$

The second term on the right-hand side of this equation is the Taylor dispersion coefficient, representing the enhancement of

axial diffusion by diffusion across the cross-hyphal velocity gradient. Because $\chi < 1$, even for moderate values of nuclear confinement the Taylor dispersion coefficient scales like χ^8. Using the parameters that we measure for real fungal hyphae ($\chi = 0.7$, $\Lambda = 0.2$), we see that the Taylor dispersion coefficient is 0.007 times smaller than if nuclei were allowed to occupy the entire hyphae and 0.3 times smaller than for an equivalent-sized capillary with no-slip walls. Dispersion within hyphae, which is the major contributor to dispersion in model capillary networks, is therefore not sufficient to deliver nuclei to growing tips at well-separated times, leading us to hypothesize that velocity variations between hyphae create the time-of-travel variance in real fungal networks.

VIII. Modeling Variation in Travel Times from the Colony Interior to the Hyphal Tips

In the main text we present a simple model for the variation in speed of a nucleus that moves through the hyphal network and whose speed varies when it passes through a hyphal junction or branch point. Specifically, the time taken to travel a distance x and velocity of the nucleus v on traveling this distance satisfy random-walk equations

$$dt = \frac{dx}{v} \quad \text{and} \quad dv = \sigma(v) dW_{x/\ell}, \tag{S14}$$

where $W_{x/\ell}$ is a Wiener process (14), ℓ is the distance traveled by the nucleus between branch or fusion points (assumed to be constant), and $\sigma(v)$ is the rms change in nuclear velocity on moving from one hypha to another. Then the joint probability density function for the particle to take time t to travel distance x and attain a velocity v on doing so, $p(x,t,v)$, satisfies a Fokker–Planck equation

$$\frac{\partial p}{\partial x} = -\frac{1}{v}\frac{\partial p}{\partial t} + \frac{1}{2\ell}\frac{\partial^2}{\partial v^2}\left(\sigma(v)^2\, p\right), \tag{S15}$$

where x is measured relative to the position of the mitotic event, and assuming that the speed of the nucleus is initially prescribed, so $p(0,t,v) = \delta(t)\delta(v - v^*)$. For given x, we are interested in computing the variance in travel times, as a function of distance traveled, i.e., $T_2 \equiv \iint t^2 p(x,t,v) dt\, dv - (\iint t p(x,t,v) dt\, dv)^2$, which gives us a measure of how far apart in time two sibling nuclei starting from the same location in the hyphae are delivered to the hyphal tips, distance x downstream. We moreover assume that the set of possible speeds is compactly supported, $v_a \le v \le v_b$, and for conservation of probability, $\frac{\partial}{\partial v}(\sigma^2 p) = 0$ for $v = v_a$ and $v = v_b$.

A. Variation in Travel Times for Large Travel Distances. To compute the asymptotic behavior of T_2 for nuclei traveling large distances through the hyphal network we use the method of moments, first introduced by Aris (15). Specifically, we define moments of the distribution p, by

$$p_n(x,v) \equiv \int \left(t - x\left\langle\frac{1}{v}\right\rangle\right)^n p(t,x,v)\, \mathrm{d}t, \tag{S16}$$

where $\langle\frac{1}{v}\rangle = \iiint \frac{1}{v} p(t,x,v)\, \mathrm{d}v\, \mathrm{d}x\, \mathrm{d}t$ is the average of the inverse velocity $1/v$. Then by direct integration of Eq. **S15** we obtain

$$\frac{\partial p_0}{\partial x} = \frac{1}{2\ell}\frac{\partial^2}{\partial v^2}\left(\sigma^2 p_0\right). \tag{S17}$$

In the limit of large x we expect that p_0 will converge to the marginal function of v; i.e., the nucleus will lose knowledge of its starting velocity, giving $p_0(v) \sim A/\sigma(v)^2$, where A is a constant that is needed to achieve the overall normalization $\int p_0(v)\, \mathrm{d}v = 1$. In this same limit $\langle\frac{1}{v}\rangle \sim \int \frac{A}{v\sigma^2}\, \mathrm{d}v$.

Multiplying Eq. **S15** by powers of $\left(t - x\langle\frac{1}{v}\rangle\right)$ and integrating, we obtain equations for higher-order moments of p:

$$\frac{\partial p_1}{\partial x} = \left(\frac{1}{v} - \left\langle\frac{1}{v}\right\rangle\right)p_0 + \frac{1}{2\ell}\frac{\partial^2}{\partial v^2}\left(\sigma^2 p_1\right) \tag{S18}$$

$$\frac{\partial p_2}{\partial x} = 2\left(\frac{1}{v} - \left\langle\frac{1}{v}\right\rangle\right)p_1 + \frac{1}{2\ell}\frac{\partial^2}{\partial v^2}\left(\sigma^2 p_2\right). \tag{S19}$$

p_1 and p_2 therefore have asymptotic forms that are also independent of x, with

$$\frac{\partial^2}{\partial v^2}\left(\sigma^2 p_1\right) \sim -2\ell\left(\frac{1}{v} - \left\langle\frac{1}{v}\right\rangle\right)p_0. \tag{S20}$$

Introduce a series of auxiliary functions $\{H_i(v)\}$ by

$$H_0(v) = \left(\frac{1}{v} - \left\langle\frac{1}{v}\right\rangle\right)\frac{A}{\sigma^2} \tag{S21}$$

$$H_i(v) = \int_{v_a}^{v} H_{i-1}(v)\, \mathrm{d}v \quad \forall i > 0; \tag{S22}$$

then as $x \to \infty$,

$$p_1(v) \sim -\frac{2\ell H_2}{\sigma^2} + \frac{B}{\sigma^2}, \tag{S23}$$

where B is a constant that contains information about the initial conditions. To determine B note that if $T_1(x) \equiv \int p_1(x,v)\, \mathrm{d}v$, then

$$\frac{dT_1}{dx} = \frac{d}{dx}\int p_1\, \mathrm{d}v = \int\left(\frac{1}{v} - \left\langle\frac{1}{v}\right\rangle\right)p_0\, \mathrm{d}v = 0. \tag{S24}$$

Thus, $T_1(x) = T_1(0) = 0$ because of our prescribed initial conditions, which requires

$$B = 2\ell A \int \frac{H_2}{\sigma^2}\, \mathrm{d}v \tag{S25}$$

and implies that the mean time for the nuclei to travel a distance x is, as we would expect, $x\langle\frac{1}{v}\rangle$.

The variance in time to travel distance x is therefore $T_2 \equiv \int p_1\, \mathrm{d}v$. Now,

$$\begin{aligned}\frac{dT_2}{dx} &= \frac{d}{dx}\int p_2\, \mathrm{d}v = 2\int\left(\frac{1}{v} - \left\langle\frac{1}{v}\right\rangle\right)p_1\, \mathrm{d}v \\ &\sim -4\ell\int\left(\frac{1}{v} - \left\langle\frac{1}{v}\right\rangle\right)\frac{H_2}{\sigma^2}\, \mathrm{d}v \\ &= -\frac{4\ell}{A}\int H_0 H_2\, \mathrm{d}v \\ &= \frac{4\ell}{A}\int H_1^2\, \mathrm{d}v,\end{aligned} \tag{S26}$$

where we integrated by parts to arrive at the final expression.

It follows that the variance in arrival times, T_2, increases linearly with distance traveled. Moreover, we can compute the functional dependence of $\sigma(v)$ upon v up to an unknown constant of proportionality by measuring the distribution of nuclear velocities at any station in the colony, because this measure-

ment gives us precisely $p_0 \propto \sigma(v)^{-2}$. Our measurements (main text, Fig. 4*B*) suggest that independently of colony size, $\sigma(v) = \sigma_0$ is approximately constant. In that case, for large x,

$$p_0(v) \sim \frac{1}{v_b - v_a} \Rightarrow$$
$$\frac{dT_2}{dx} = \frac{4\ell}{\sigma_0^2}\left(\frac{1}{3}\frac{v_b^2 + v_a v_b + v_a^2}{(v_b - v_a)^2}\log\left(\frac{v_b}{v_a}\right)^2 - \frac{3}{2}\frac{v_a + v_b}{v_b - v_a}\log\left(\frac{v_b}{v_a}\right) + 2\right), \quad \textbf{[S27]}$$

which yields Eq. **4** from the main text in the limit $v_a \ll v_b$.

B. Variation in Travel Times for Small Travel Distances. For nuclei not traveling far from their starting locations, we can compute the dependence of T_2 upon distance x, conditioned on the nuclear starting velocity v^*, by making a formal series expansion in powers of x of the solution to Eq. **S15**:

$$p(x,t,v) \sim \sum_n \frac{x^n}{n!}\tilde{p}_n(t,v), \text{ where } \tilde{p}_n \equiv \left(-\frac{1}{v}\frac{\partial}{\partial t} + \frac{1}{2\ell}\frac{\partial^2}{\partial v^2}\sigma^2\right)\delta(t)\delta(v - v^*). \quad \textbf{[S28]}$$

Then

$$T_1(x) \equiv \iint tp(x,t,v)\, dtdv \sim \frac{x}{v^*} + \frac{x^2\sigma(v^*)^2}{2\ell v^{*3}} + o(x^2) \quad \textbf{[S29]}$$

and

$$T_2(x) \equiv \iint t^2 p(x,t,v)\, dtdv - T_1(x)^2$$
$$\sim \frac{x^2}{v^{*2}} + \frac{4x^3\sigma(v^*)^2}{3\ell v^{*4}} - T_1(x)^2 + o(x^3) \sim \frac{x^3\sigma(v^*)^2}{3\ell v^{*4}} + o(x^3). \quad \textbf{[S30]}$$

To compute the total expected variability in travel times, we must multiply by the marginal probability for the start velocity v^*, computed in the previous section as $p_0(v^*) = A/\sigma(v^*)^2$, and obtain

$$\mathbb{E}(T_2(x)) = \int T_2(x)p_0(v^*)\, dv^* \sim \frac{Ax^3}{9\ell}\left(\frac{1}{v_a^3} - \frac{1}{v_b^3}\right). \quad \textbf{[S31]}$$

Note that, unlike the long time dispersion in arrival times, this quantity does not depend explicitly on the function $\sigma(v)$, except through the constant of normalization A. There is thus limited scope for the fungus to optimize mixing over short distances by manipulating $\sigma(v)$.

1. Ramos-García SL, Roberson RW, Freitag M, Bartnicki-García S, Mouriño-Pérez RR (2009) Cytoplasmic bulk flow propels nuclei in mature hyphae of *Neurospora crassa*. *Eukaryot Cell* 8(12):1880–1890.
2. Martegani E, Levi M, Trezzi F, Alberghina L (1980) Nuclear division cycle in *Neurospora crassa* hyphae under different growth conditions. *J Bacteriol* 142(1): 268–275.
3. Ryan FJ, Beadle G, Tatum E (1943) The tube method of measuring the growth rate of *Neurospora*. *Am J Bot* 30(10):784–799.
4. Fleissner A, et al. (2005) The so locus is required for vegetative cell fusion and postfertilization events in *Neurospora crassa*. *Eukaryot Cell* 4(5):920–930.
5. Ruiz-Roldán MC, et al. (2010) Nuclear dynamics during germination, conidiation, and hyphal fusion of *Fusarium oxysporum*. *Eukaryot Cell* 9(8):1216–1224.
6. Korolev KS, Avlund M, Hallatschek O, Nelson DR (2010) Genetic demixing and evolution in linear stepping stone models. *Rev Mod Phys* 82(2):1691–1718.
7. Crow JF, Kimura M (1970) *An Introduction to Population Genetics Theory* (Harper & Row, New York).
8. Sveen J (2004) *Mechanics and Applied Mathematics* (Department of Mathematics, University of Oslo, Oslo), Technical Report Eprint no. 2.
9. Crocker JC, Grier DG (1996) Methods of digital video microscopy for colloidal studies. *J Coll Int Sci* 179:298–310.
10. Atwood KC, Mukai F (1955) Nuclear distribution in conidia of *Neurospora* heterokaryons. *Genetics* 40(4):438–443.
11. Saffman P (1959) A theory of dispersion in a porous medium. *J Fluid Mech* 6:321–349.
12. Lauga E, Brenner M, Stone H (2007) Microfluidics: The no-slip boundary condition. *Handbook of Experimental Fluid Dynamics*, eds Tropea C, Yarin A, Foss J (Springer, Berlin), pp 1219–1240.
13. Taylor G (1953) Dispersion of soluble matter in solvent flowing slowly through a tube. *Proc R Soc Lond A* 219(1137):186–203.
14. Gardiner C (1985) *Handbook of Stochastic Methods for Physics, Chemistry and the Natural Sciences, Series in Synergetics* (Springer, Berlin).
15. Aris R (1956) On the dispersion of a solute in a fluid flowing through a tube. *Proc R Soc Lond A* 235(1200):67–77.

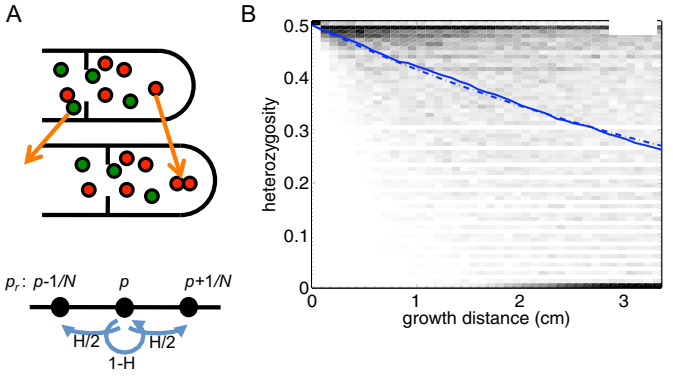

Fig. S1. (*A*) In most filamentous fungi, a small apical population of nuclei is sufficient to feed each growing tip by mitosis. Supposing no mixing between populations supplying different tips, we model the decrease in genomic richness in this small population by a Moran process, one step of which is shown: In an increment of growth x_g/N, one nucleus produces two clonal offspring, and another nucleus is removed from the apical population (birth and migration out of the apical tip are shown by arrows). (*B*) The richness (heterozygosity) of a small nuclear population is expected to decrease exponentially with the distance grown by the hyphal tip. We simulated 500 hyphal tips starting with equal numbers of red and green-labeled nuclei: $(n_r, N) = (65, 130)$. The grayscale plot shows the composition (heterozygosity, *H*) of all 500 hyphal tips (black, most hyphal tips; white, fewest). In a substantial fraction of tips (81/500, after 3 cm of growth), $H \to 0$; i.e., one or the other of the populations becomes totally extinct. The solid blue curve is the mean heterozygosity for all 500 hyphal tips and the dotted line is the predicted decay in heterozygosity $H(x) = H(0)\exp(-2x/Nx_g)$, where x_g is the distance grown by the colony in a single generation: $x_g \approx 0.84$ mm.

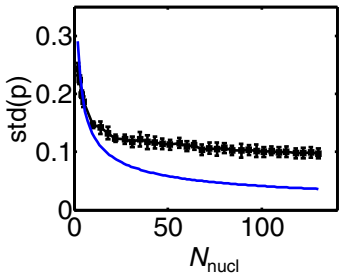

Fig. S2. std(p_r) is an index of mixing quality in a chimeric colony. Black: Dependence of std(p_r) on the number of nuclei in each sample (N_{nucl}). Data from a 2-cm mycelium are shown. Error bars: SE from four replicate colonies. Blue: Simulated dependence of std(p_r) upon N_{nucl}, in the limit of perfect mixing ($\langle p_r \rangle$ matched to the real data, and each nucleus assigned its nucleotype independently and at random).

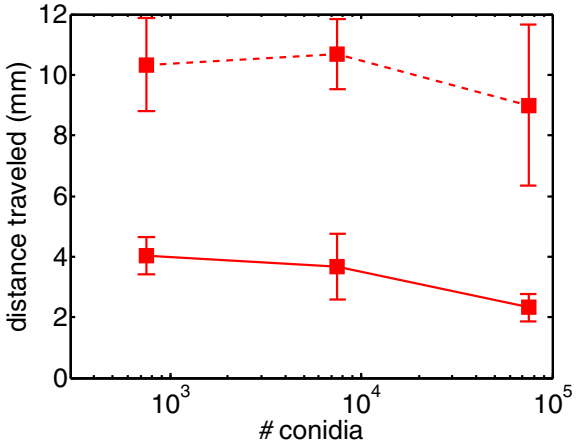

Fig. S3. By varying the concentration of the spore inoculum, we checked that the wt colony architecture and dispersal of hH1-GFP nuclei is not affected by the number of *hH1-gfp* spores introduced into the colony. We report both the maximal distance traveled by the nuclei (dashed line) and the mean distance (solid line) in 1 h (mean *pm* SD from three replicates).

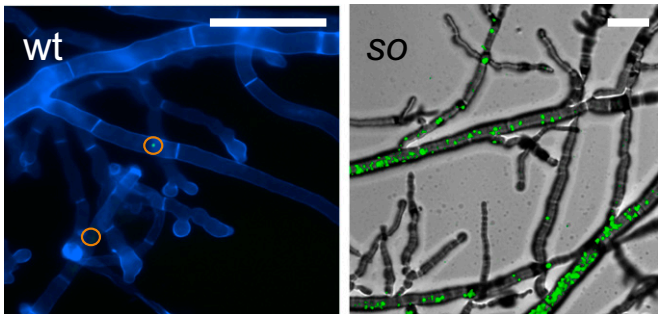

Fig. S4. Nuclei introduced into either wild-type or *so* colonies disperse at the same rate from their sites of introduction to the growing hyphal tips of the colony. However, in wild-type colonies (*Left*, hH1-GFP nuclei in a calcofluor-stained colony), nuclei (circled in orange) become spread apart during their passage through the colony. In *so* colonies (*Right*, hH1-GFP nuclei in a colony imaged in DIC), nuclei move as a coherent raft, suggesting that sibling nuclei do not arrive at the growing front well separated in time. (Scale bars, 50 μm.)

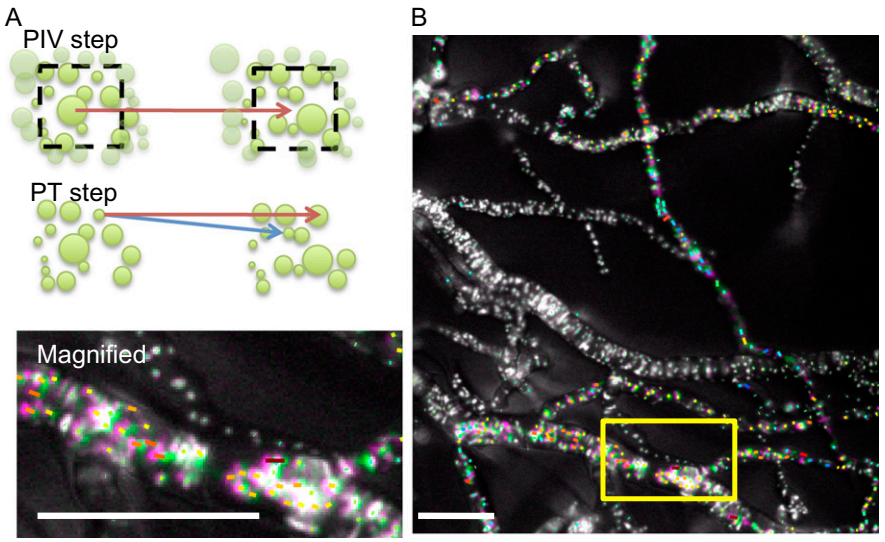

Fig. S5. By hybridizing PIV and PT methods we are able to simultaneously measure the spatially complex velocities of several thousand nuclei within a single imaging field. (*A*) Scheme of how PIV and PT methods are used to track nuclear dispersal. A PIV step measures the mean velocity of groups of nuclei (black dashed box) whose motions are coordinated. However, nuclei also move within groups. Because reorganization of nuclei within groups also contributes to mixing, we then implement a second particle-tracking step: Nuclei are located and morphologically categorized. The position of each nucleus is extrapolated to the next frame (red arrow), and then the corresponding closest-matching nucleus (based on Eq. **S1**) is identified by a greedy algorithm (blue line). (*B*) A single frame of real PIV/PT data. Shown are reconstructed nuclear displacements over 0.2 s, from a 0.3 × 0.3-mm field (real imaging fields were 0.7 × 0.7 mm). We show two consecutive frames in the magenta and green color channels. Moving nuclei show up as pairs of spots, one magenta and the other green. Lines are color coded by nuclear velocity. (*Left*) Magnified region shown by yellow rectangle in the *Right* image. (Scale bars, 50 μm.)

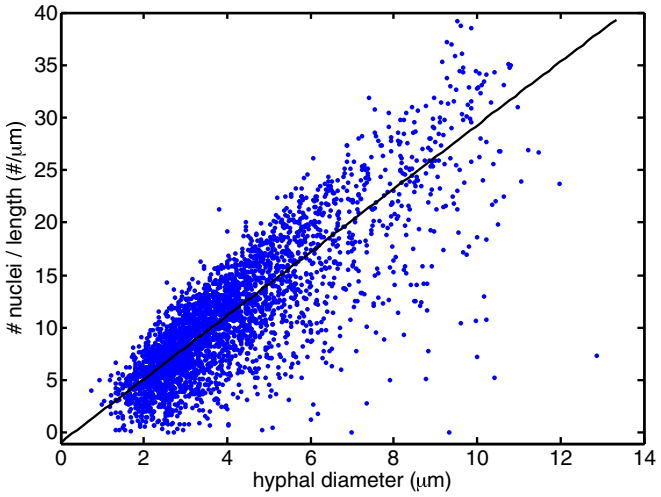

Fig. S6. Number density of nuclei, i.e., number of nuclei counted in unit length of hypha, increases in proportion to the hyphal diameter. Blue circles represent nuclear number densities of 3,300 hyphae, including hyphae at the edge of the colony, and 8 mm behind the colony edge. The black curve is the line of best fit, whose equation is number density (μm^{-1}) = 3.02 (μm^{-2}) × diameter − 0.92 (μm^{-1}).

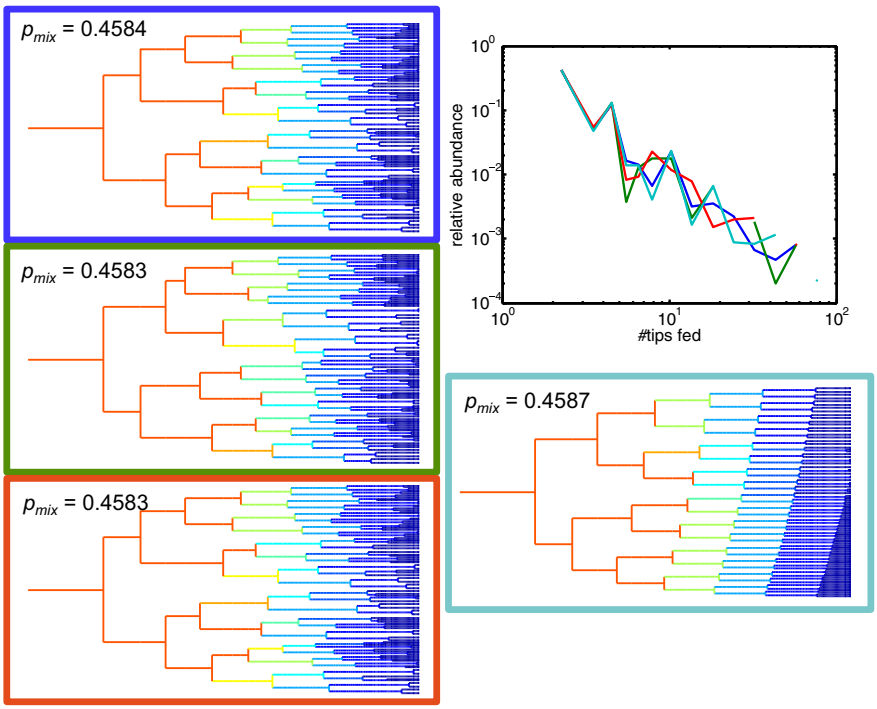

Fig. S7. Optimization of p_{mix} produces multiple, nearly optimally branching but nonisomorphic trees with similar values of p_{mix}. (*Left*) Geometry of three trees, each with 100 hyphal tips, that have close to p_{mix} within 0.05% of its minimal value, compared with the optimal branching geometry (*Lower Right*). (*Upper Right*) Nonisometry of trees is seen by plotting the distribution of the number of tips fed by each hypha (colors of probability distribution curves match the outline colors for the geometry plots). Minimization of p_{mix} strongly constrains the lengths and relative numbers of hyphae feeding 1, 2, or 3 tips, i.e., the branching points closest to the colony periphery, but allows considerable freedom in the location of branch points in the colony interior.

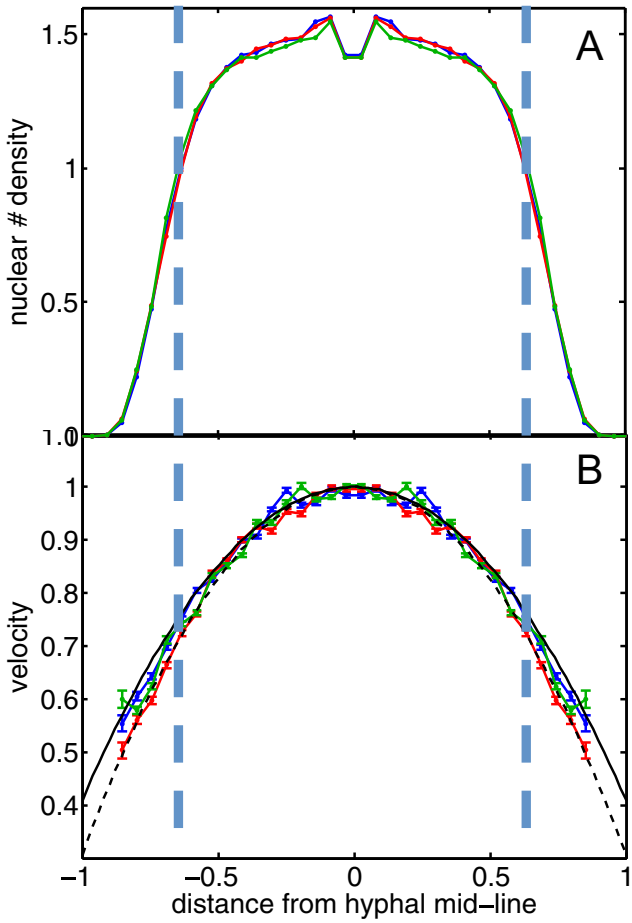

Fig. S8. Average nuclear velocities across hyphal cross-sections are parabolic, a signature of Poiseuille or pressure-driven flow, universally between hyphae and colonies of different ages, once velocities are scaled by the velocity on the hyphal centerline and distances from this centerline are scaled by the hyphal radius. Colors denote data from colonies of different sizes: blue, 3 cm; green, 4 cm; and red, 5 cm [$(N_{nucl}, N_{hyph}) = (341{,}381,\ 887)$, $(352{,}428,\ 879)$, and $(266{,}384,\ 737)$ respectively]. However, nuclei are confined to the central portion of the hypha (70% of the total hyphal width). (*A*) The number of nuclei detected vs. distance from centerline. (*B*) Average velocities of those nuclei. Error bars: SE in velocity measurement. Additionally, there is apparent slip on the hyphal walls, so that nuclear velocities, when extrapolated to the wall, do not vanish there. Black curves are best-fit estimates of the slip length Λ (solid curve, $\Lambda = 0.3$; dashed curve, $\Lambda = 0.2$).

Table S1. Proportions of spores and colonies categorized as hH1-GFP homokaryotic, hH1-dsRed homokaryotic, or heterokaryotic (containing nuclei of both nucleotypes)

Nucleotypes	Conidial identity, n = 1,032	Colony identity, n = 102
hH1-GFP	0.29	0.35
hH1-dsRed	0.11	0.12
Heterokaryotic	0.60	0.53

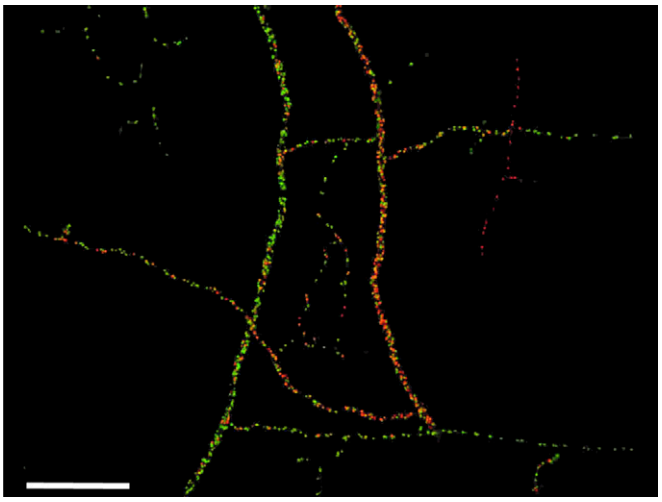

Movie S1. (*S1-heterokaryon.mov*.) Sequence of confocal laser scanning microscope (CLSM) images of hH1-DsRed and hH1-GFP nuclei moving around within a single fungal mycelium. Capture rate is one frame per 7 s. Movie plays at 175 × real speed. (Scale bar, 100 μm.)

Movie S1

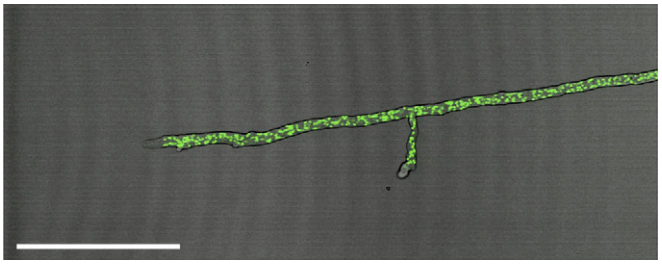

Movie S2. (*S2-nuclflowneartip-sm.mov*.) Sequence of CLSM (and simultaneous bright field) images of hH1-GFP nuclear flow near the tip of a colony. Original capture rate is one frame per second. Movie plays at 10 × real speed. (Scale bar, 100 μm.)

Movie S2

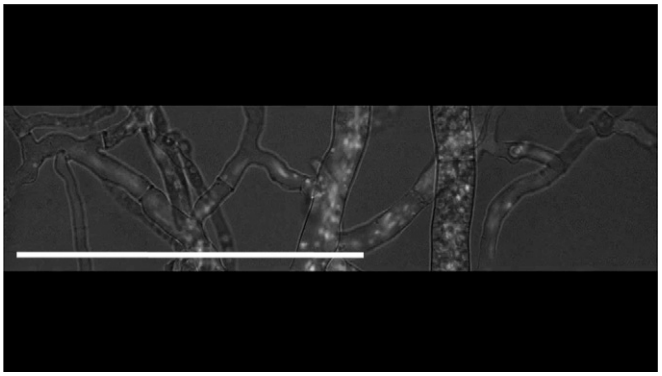

Movie S3. (*S3-mixingflows-sm.mov*.) CLSM image sequence of nuclear flows near the periphery of a 5-mm × 25-mm *Neurospora* colony. Capture frame rate is 7.5 frames per second. Movie plays at 3.5 × real speed. (Scale bar, 100 μm.)

Movie S3

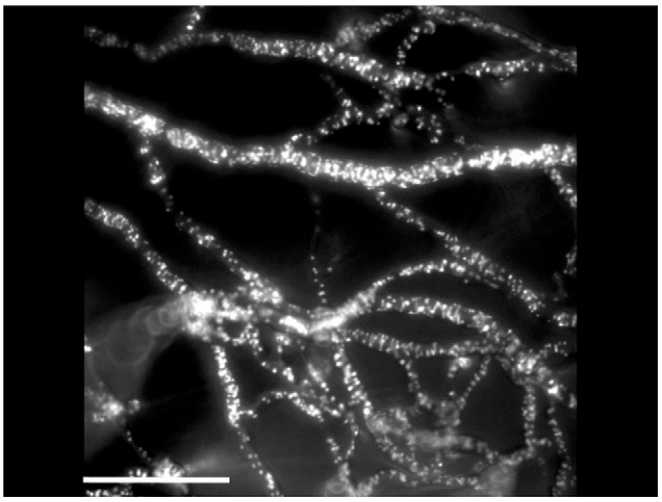

Movie S4. (*S4-flowreversal.mov*.) Flow is reversed when colonies are exposed to hyperosmotic treatments (forward and reverse segments are individually looped, around 10 s of real time footage). Imaged region is ~8 mm from the growing edge of a 3-cm colony. Capture frame rate is five frames per second. Movie plays at 6 × real speed. (Scale bar, 100 μm.)

Movie S4